HHS Public Access

Author manuscript

Oncogene. Author manuscript; available in PMC 2017 June 12.

Published in final edited form as:

Oncogene. 2017 May 25; 36(21): 3025–3036. doi:10.1038/onc.2016.456.

Emergent Role of the Fractalkine Axis in Dissemination of Peritoneal Metastasis from Epithelial Ovarian Carcinoma

Hilal Gurler Main[1], **Jia Xie**[1], **Goda G. Muralidhar**[1], **Osama Elfituri**[2], **Haoliang Xu**[2], **Andre A. Kajdacsy-Balla**[2], and **Maria V. Barbolina**[1,#]

[1]Department of Biopharmaceutical Sciences, University of Illinois at Chicago, Chicago, IL 60091

[2]Department of Pathology, University of Illinois at Chicago, Chicago, IL 60091

Abstract

Epithelial ovarian carcinoma is the most common cause of death from gynecologic cancers largely due to advanced, relapsed, and chemotherapy-resistant peritoneal metastasis, which is refractory to the currently used treatment approaches. Mechanisms supporting advanced and relapsed peritoneal metastasis are largely unknown, precluding development of more effective targeted therapies. In this study we investigated the function of a potentially targetable fractalkine axis in the formation and the development of advanced and relapsed peritoneal metastasis and its impact on patients' outcomes. Our mouse model studies support a role for the fractalkine receptor (CX_3CR1) in the initiation of peritoneal adhesion important for recolonization of relapsed peritoneal metastasis. We show that downregulation of CX_3CR1 results in reduction of metastatic burden at several peritoneal sites commonly colonized by advanced and relapsed metastatic ovarian carcinoma. We show that the chemokine fractalkine (CX_3CL1), an activating ligand of CX_3CR1, regulates organ-specific peritoneal colonization. High expression of CX_3CR1 correlates with significantly shorter survival, specifically in post-menopausal patients with advanced and terminal stages of the disease. Taken together, our studies support a key regulatory role for the fractalkine axis in advanced and relapsed peritoneal metastasis in epithelial ovarian carcinoma.

Keywords

ovarian carcinoma; fractalkine; fractalkine receptor; metastasis

Introduction

Advanced, relapsed, and chemotherapy-resistant metastatic epithelial ovarian carcinoma is a major clinical challenge, because the currently used treatment approaches, mainly consisting of surgery and cytotoxic chemotherapy, fail to cure the disease at these terminal stages. For

#Corresponding Author: Maria V. Barbolina, PhD, 833 South Wood Street, Chicago, IL 60612, phone: 312-355-0670, fax: 312-996-0098, mvb@uic.edu.

Conflict of interest

All authors declare no conflict of interests.

Supplementary information accompanies the paper on the *Oncogene* website (http://www.nature.com/onc).

the past several decades epithelial ovarian carcinoma, of which high grade serous is the most predominant and deadliest histotype, was the leading cause of mortality from gynecologic malignancies and the fifth cause of death from all cancers affecting women; only in the US more than 15,000 women die annually from this disease (1–7). To improve survival it is imperative to develop new treatment approaches that specifically target the metastatic disease. To this end, identification of the mechanisms that promote metastatic success of ovarian carcinoma could yield better targets for the development of novel therapeutics.

The majority of ovarian carcinoma patients are first diagnosed when peritoneal metastases have already spread (8, 9). In patients with metastatic disease progression from the time of the initial diagnosis to death is often very quick; according to current statistics, the 5-year survival for this cohort is less than 30%. Initial peritoneal lesions as well as recolonization by the recurrent disease occur as a result of lodging the malignant cells shed from the primary tumor on to peritoneal mesothelium, the lining of the peritoneum that consists of parietal peritoneum and visceral peritoneum continuous with each other. Once the disseminating cells have successfully adhered to the mesothelium, they invade the submesothelial matrix and establish secondary lesions in the stroma of intraperitoneal tissues and organs. Patients diagnosed with disseminated ovarian carcinoma undergo surgery, including hysterectomy, bilateral salpingo-oophorectomy, omentectomy, and debulking of peritoneal metastasis; however, complete tumor resection often cannot be achieved (10–12). Moreover, cytotoxic chemotherapy regimens to which patients are subjected fail to eliminate all tumor cells due to acquired and intrinsic resistance to chemotherapy (13–16). Consequently, metastases often recur in the peritoneal wall and other remaining peritoneal organs. The microenvironment at these secondary sites likely supports organ-specific colonization, although the underlying mechanisms are not well understood (17). Uncontrolled proliferation of metastatic lesions leads to their expansive growth, which eventually causes death through malnutrition and bowel obstruction.

Hence, peritoneal adhesion and metastatic cell proliferation are among the key processes in the metastatic cascade of ovarian carcinoma that could be exploited for anti-metastatic intervention by novel targeting agents.

Targeted therapies directed against tumor-specific pathways and molecules have been more successful in treating metastasis compared to the conventional cytotoxic chemotherapy (18). We reasoned that the chemokine family G protein-coupled receptor fractalkine (CX_3CR1) might be such a molecule, because it is expressed in 64% of metastatic ovarian carcinoma specimens (19) and *in vitro* studies showed that CX_3CR1-positive ovarian carcinoma cells adhered to mesothelial monolayer and proliferated in CX_3CL1-dependent manner (19, 20); moreover, we previously reported that CX_3CR1 was expressed in all tested types of stromal and epithelial ovarian carcinoma (19, 21, 22). Chemokine receptors are seven transmembrane G protein-coupled receptors (GPCR) that are activated upon ligand (chemokine) binding resulting in activation of intracellular signaling networks that regulate processes vital for both normal and cancer cells (23–25). Approximately 50% of all currently used drugs are directed against GPCRs, underscoring their value as successful drug targets (26). Fractalkine receptor is uniquely and specifically activated by the only ligand, the chemokine CX_3CL1 (fractalkine) (27, 28). CX_3CL1 is a unique member of the CX_3C

subfamily of chemokines, as it contains a transmembrane domain with which it anchors on the cell membrane and supports cell-cell adhesion. Proteolytic cleavage of CX_3CL1 yields a soluble form capable of inducing cell migration and proliferation (29–31). CX_3CL1 is expressed by epithelial ovarian carcinoma cells and it can be detected in malignant ascites from patients (19, 20), but its expression status across the peritoneal organs and tissues serving as metastatic sites is largely unknown. The fractalkine axis has previously been shown to regulate adhesion and migration of leukocytes and signaling from neurons to glia (29, 32). Notably, a role in supporting metastatic colonization of breast, prostate, and pancreatic cancers has also been established (33–36). Due to the prominent role of CX_3CR1 in various pathological conditions extensive efforts have been invested to design and develop CX_3CR1 inhibitors. Such inhibitors have proven specific and effective in the pre-clinical setting (37–39), providing a strong rationale for potential CX_3CR1-directed therapies in ovarian carcinoma.

Here we build on our *in vitro* mechanistic studies (19) and show that in patients and in a syngeneic mouse model expression of CX_3CR1 strongly correlates with mortality and metastatic development at CX_3CL1-positive peritoneal organs. Our data validate CX_3CR1 as a potential therapeutic target in late-stage metastatic ovarian carcinoma.

Results

Status of CX_3CR1 expression predicts survival of patients with serous EOC

Our previous studies suggested that the CX_3CL1/CX_3CR1 axis supports cell-cell adhesion, migration, and proliferation (19), all of which are essential for successful colonization and metastatic expansion. These properties are directly linked to the aggressiveness of cancer metastasis; however, the relationship between expression of CX_3CR1 and patients' survival has not yet been investigated. We used gene expression data from The Cancer Genome Atlas (TCGA) database for serous ovarian adenocarcinoma (n=557) and the Oncomine platform (40). We found that patients' survival inversely correlated with the level of CX_3CR1 expression (FIGURE 1A, left panel). Moreover, patients with high CX_3CR1 expression lived significantly shorter compared to their counterparts with low CX_3CR1 expression (FIGURE 1A, center panel). Furthermore, we asked whether CX_3CR1 expression status correlated with survival of patients at advanced and terminal FIGO stages. We divided specimens in three groups, including those at The International Federation of Gynecology and Obstetrics (FIGO) Stage I and II, III, and IV (Supplementary FIGURE 1A). In the group containing patients with Stage III disease, those with high CX_3CR1 expression survived significantly shorter compared to the patients with low CX_3CR1 expression (FIGURE 1B, left and right panels). For patients with Stage IV disease the difference in survival as a function of CX_3CR1 expression was even more pronounced, as patients with high CX_3CR1 lived twice shorter compared to those with low CX_3CR1. In fact, all patients with Stage IV disease and high CX_3CR1 expression died by a little over 2000 days, while at least one third of patients with Stage IV disease and low CX_3CR1 expression were still alive at this time point (FIGURE 1B, center and right panels). As ovarian carcinoma is associated with age, we also asked whether menopausal status in a combination with CX_3CR1 expression played a role in survival. To address this, the specimens were divided into pre- and post-menopausal groups

(Supplementary FIGURE 1B). Interestingly, in the pre-menopausal cohort CX_3CR1 expression did not affect survival (FIGURE 1C, left and right panels). In contrast, in post-menopausal patients' cohort, high CX_3CR1 expression significantly correlated with worse survival compared to the patients with low CX_3CR1 expression (FIGURE 1C, center and right panels). Thus, not only that patients with high expression of CX_3CR1 survived significantly shorter than those with low CX_3CR1 expression, this decrease in survival was significantly more pronounced in post-menopausal patients at terminal stages of the disease. These data suggest that high expression of CX_3CR1 in primary ovarian carcinoma, occurring in a quarter of the tested patients' population, is a predictor of worse survival for the late stage post-menopausal women with serous epithelial ovarian cancer.

Downregulation of the CX_3CR1 expression reduces peritoneal adhesion and metastasis formation in a syngeneic model of ovarian cancer

Analysis of patients' survival indicated that high expression of CX_3CR1 correlated with shorter survival (FIGURE 1) and previous *in vitro* studies have suggested a role of CX_3CR1 in CX_3CL1-dependent peritoneal adhesion and proliferation (19, 20); however, this did not explain whether CX_3CR1 played an active role in aggressiveness of the disease or simply correlated with its progression. To test this, we employed the ID8/C57BL/6 syngeneic mouse model of ovarian carcinoma to determine the role of tumoral CX_3CR1 in the disease progression in the presence of a functional immune system. ID8 has been derived by spontaneous transformation of the murine ovarian epithelium and, thus, provides a model to study metastatic dissemination in the presence of the native immune system (41); however, it has been recently shown that ID8 does not carry mutations in TP53 and in other genes commonly mutated in ovarian carcinoma (42). We reasoned that CX_3CR1-directed therapies may not be able to affect all of the CX_3CR1-positive cells and/or may not be able to completely block CX_3CR1 activity in the context of the involved organs due to various complications, including drug permeability and its intratumoral concentration. To better model such a scenario, we created ID8 clones in which CX_3CR1 was downregulated rather than completely knocked-out. These clones were generated by transfecting a pool of four CX_3CR1-specific shRNAs following puromycin selection. Downregulation of CX_3CR1 of an average of 30% was confirmed by Western blot and immunofluorescence staining in four subclones, termed cx2, cx3, cx4, and cx6 (Supplementary FIGURE 2A,B). Significant reduction of CX_3CR1-dependent cell proliferation and migration in the selected clones was confirmed using Transwell cell migration and proliferation assays, confirming the loss of function as a consequence of reduction of CX_3CR1 expression. Non-effective 29-mer scrambled shRNA cassette in retroviral untagged vector and an empty untagged vector were used to create control cell lines (designated "scr sh" and "vector", respectively), in which neither CX_3CR1 expression nor CX_3CL1-dependent cell migration and proliferation were significantly altered compared to the parental ID8 (Supplementary FIGURE 2C,D). Further, a small molecule specific inhibitor of CX_3CR1, compound 18a (37), was able to efficiently block CX_3CL1-mediated cell proliferation (Supplementary FIGURE 3).

To determine the requirement of CX_3CR1 in peritoneal adhesion we used a short-term *in vivo* adhesion assay. Prior to i.p. injection both control (ID8 and scr sh) and experimental (cx2 and cx4) cells were transfected with GFP. Following i.p. injection of GFP-labeled cells

into abdomens of C57BL/6 mice the intraperitoneal adhesion was allowed to take place for 4 hours. Adhered ovarian carcinoma cells were found mainly on the surfaces of omentum and anterior peritoneal wall, consistent with the pattern of metastatic seeding of early peritoneal metastasis. Experimental groups showed significantly reduced number of adhered cells compared to the controls (FIGURE 2A), further supporting a key role of the fractalkine axis in peritoneal adhesion of ovarian carcinoma cells.

To determine the impact of reduction of peritoneal adhesion on tumor formation we i.p. injected both control (ID8 and scr sh) and experimental (clones cx2, cx3, and cx6) cells into abdomens of C57BL/6 mice and allowed animals to reach humane endpoints. Downregulation of CX_3CR1 expression resulted in a significant reduction of the number of animals bearing tumors at all peritoneal mesothelial surfaces, such as parietal peritoneum and visceral peritoneum (FIGURE 2B). These data suggest that impairment of peritoneal adhesion via downregulation of CX_3CR1 could result in reduction of metastasis formation.

To validate our findings in human-derived mesothelial cell lines we measured CX_3CL1 expression in human mesothelium from healthy donors. All specimens of female visceral peritoneum containing mesothelial cells (n=5) displayed very strong (nearly 3+) immunoreactivity against CX_3CL1 antibodies in mesothelial cells (FIGURE 2C; Supplementary TABLE 1), suggesting that CX_3CL1/CX_3CR1-dependent peritoneal adhesion may occur in human disease.

Downregulation of CX_3CR1 expression reduces metastatic burden in a syngeneic model of ovarian cancer

Previous findings indicating a role of CX_3CL1/CX_3CR1 in ovarian carcinoma cell proliferation prompted us to examine the effect of downregulation of CX_3CR1 on the tumor burden in the ID8/C57BL/6 syngeneic mouse model. We analyzed the overall tumor burden and found that the total tumor volume and size for all experimental groups (cx2, cx3, and cx6) was significantly lower than that for the control groups (ID8 or scr sh; FIGURE 3A,B), suggesting that expression of CX_3CR1 is tightly linked to tumor burden possibly via supporting CX_3CL1-dependent cell proliferation. Importantly, expression of CX_3CR1 in the clone cells (score 3+) remained lower than in the parental ID (score 2+) at the end of the experiments (FIGURE 3C). Moreover, parental cells displayed strong Ki67 and PCNA staining (3+) compared to the cx2 clone cells (2+), suggesting that proliferation of clone cells with reduced CX_3CR1 expression remained lower than in the parental cells throughout the experiment. Reduced proliferation in the clone cells was accompanied by the evidence of apoptosis, as determined by staining with CD95 (score 1+), while the parental ID8 cells were not undergoing apoptosis, as these tissues scored negatively for CD95 staining (FIGURE 3D).

Next, to evaluate the role of the fractalkine signaling in organ-specific tumor growth we analyzed distribution of the tumor burden by site. Interestingly, tumor burden at sites covered by the parietal peritoneum, such as the anterior and the posterior peritoneal wall and diaphragm, was significantly reduced when CX_3CR1 in the cancer cells was downregulated (FIGURE 4A). Tumor burden on liver, covered by the visceral peritoneum, was also reduced in response to downregulation of CX_3CR1 (FIGURE 4B). However, growth of tumors

underlying the mesentery anchored in small intestines was not affected by reduction of CX_3CR1 expression (FIGURE 4C). Similarly, although average tumor burden in one of the experimental groups (cx2) was nearly statistically significantly lower compared to the control scrsh group (p=0.064), overall, omental tumors in both control and experimental conditions did not significantly differ in size when animals have reached moribund conditions (FIGURE 4D). However, complete omentectomy is the standard of care for patients undergoing surgery for ovarian carcinoma; hence, management of the relapsed disease will not be complicated by the omental metastasis. We also assessed tumor formation at retroperitoneal sites, and found that downregulation of CX_3CR1 did not affect tumor burden at pancreas, whereas it significantly reduced it at the kidney (FIGURE 5). These data indicate that growth of the CX_3CR1-expressing ovarian carcinoma cells depends on the context of the host tissue.

It is important to note that these animal model studies were designed to determine the role of CX_3CR1 in tumor growth rather than survival. Paracentesis was not performed; instead, animals were sacrificed when they became moribund, resulting in comparable survival among the control and experimental groups (Supplementary FIGURE 4A). Volumes of ascites did not significantly vary among all groups (Supplementary FIGURE 4B) and lymph node tissues were CX_3CL1-negative (Supplementary FIGURE 4C, Supplementary TABLE 2), indicating that CX_3CL1/CX_3CR1 does not contribute to ascites formation.

Expression of CX_3CL1 in intraperitoneal organs targeted by metastatic dissemination correlates with tumor growth of CX_3CR1-positive cells

Previous studies suggested that once ovarian carcinoma cells attach to the mesothelial monolayer, they disrupt it by invading between the intercellular spaces followed by establishing secondary lesions in submesothelial stroma (43, 44). Hence, interaction with the matrix and cells lying beneath the mesothelium could become more important for cell proliferation and growth of metastasis than the initial interaction of metastasizing ovarian carcinoma cells with the mesothelial cells. The local microenvironment surrounding invading metastatic cells varies according to the host site; consequently, the paracrine signaling regulating proliferation of peritoneal metastases could be driven by different growth factors. As downregulation of CX_3CR1 affected tumor growth at peritoneal wall, diaphragm, liver, and kidney, we hypothesized that cell proliferation at these sites largely depended on fractalkine signaling. High levels of CX_3CL1 expression at these would be consistent with such a model of CX_3CL1-dependent proliferation. On the other hand, tumor formation at omentum, pancreas, and small intestine did not depend on CX_3CR1, indicating that tumor cell proliferation at these sites is regulated by other growth factors. Indeed, Western blot analysis showed low expression of CX_3CL1 in omentum and pancreas, while the peritoneal wall and diaphragm had comparatively high expression levels. Major immunoreactive bands with apparent molecular weight of about 55 kDa were observed in both the control and tested specimens (FIGURE 6A), confirming previously reported findings in pancreas (45). Further, using immunohistochemistry we identified that both tumor and host tissues were CX_3CL1-positive (FIGURE 6B,C). However, the intensity of CX_3CL1 immunostaining in skeletal muscle cells of diaphragm (100% of cells, score 2+) and tubular cells of kidney (100% of cells, score 3+) was stronger than that in the tumor

itself (score 1+; FIGURE 6B). On the other hand, both host tissues and tumors developed at pancreas and omentum had similar intensity of CX_3CL1 immunostaining (FIGURE 6C). These findings could argue in favor of a significant role of host CX_3CL1 in supporting the growth of peritoneal lesions seeded by CX_3CR1-positive ovarian cancer cells in our mouse model. These data also suggest that the role of tumoral CX_3CL1 in metastatic cell growth is minimal; additionally, analysis of CX_3CL1 expression in human serous ovarian carcinoma specimens showed a weak correlation with CX_3CR1 expression and no correlation between its expression levels and patients survival (Supplementary FIGURE 5). In contrast, recent studies suggest a prominent role for the autocrine fractalkine signaling in colorectal carcinoma, as tumor cells that co-expressed both CX_3CR1 and CX_3CL1 did not disseminate leading to reduced metastasis and longer survival (46). Perhaps, distinct modes of metastatic dissemination and intertumoral differences may result in dissimilar outcomes related to the role of the fractalkine axis in advanced and relapsed metastasis from different cancer types. Additionally, the level of CX_3CR1 reduction in our model may not have been sufficient to affect tumor formation at other organs, such as omentum, in which case only animals in cx2 group showed trends toward reduced omental tumor burden.

To determine the relationship between CX_3CL1 expression in peritoneal tissues and the propensity for hosting metastatic ovarian carcinoma cells in human subjects, we analyzed its expression in a subset of normal peritoneal tissues serving as hosts for metastasis. We conducted immunohistochemistry using specimens of two normal human tissues, liver and kidney, dissemination to which was CX_3CR1-dependent in the mouse model. These tissues were characterized by high intensity of CX_3CL1 immunostaining, which was detected on the cell membrane, the cytoplasm, and the nucleus (FIGURE 7A, Supplementary TABLES 3 and 4). Nearly 100% of hepatocytes and 100% of Kupffer cells in the liver tissue were strongly CX_3CL1-positive (average score in female specimens 2.6+). Distal tubular cells of kidney were strongly CX_3CL1-positive (score 3+), while CX_3CL1 expression in proximal tubular cells of kidney and interstitial stromal cells was lower (score 1+); in total CX_3CL1 score in kidney averaged to 2.4+. In the specimens of intestine/colon and omentum, dissemination to which was not CX_3CR1-dependent in the mouse model, CX_3CL1 immunoreactivity localized to sparsely present fibroblasts and endothelial cells and it was predominantly nuclear (FIGURE 7B, Supplementary TABLE 1). Average immunoscores for kidney and liver were significantly higher compared to those for intestine/colon (FIGURE 7C), suggesting that in patients, proliferation of lesions lodged on liver and kidney could, to a large extent, depend on CX_3CL1 expressed in these tissues.

Discussion

Our studies suggest that the fractalkine axis actively contributes to the development of both initial and recurrent ovarian carcinoma metastasis at several crucial points, including peritoneal adhesion and tumor formation as well as organ-specific colonization and growth of tumor lesions, ultimately impacting patient survival. However, the ID8 cell line has now been extensively characterized (42) and it does not have mutational patterns characteristic of human ovarian cancers and in particular does not have a TP53 mutation which is pathognomonic of high grade serous ovarian cancers. Thus the relevance of the current

studies to human ovarian cancers will need to be determined from studies of additional relevant murine models and of human ovarian cancer samples.

We show that downregulation of CX_3CR1 impairs peritoneal adhesion and reduces formation of tumor lesions in a syngeneic model of the disease. Peritoneal adhesion is a key event for both the development of initial metastatic lesions and recolonization of the abdominal tissues by the recurrent disease. The role of the fractalkine axis in *de novo* formation of ovarian carcinoma metastasis seems to parallel that previously described in cancers of other primary sites, including breast and pancreatic carcinomas (33–35). Our findings suggest that in recurrent metastatic disease, recolonization of the abdomen could be, at least partially, prevented and blocked if the fractalkine axis is inactivated.

Our findings suggest a prominent role for the CX_3CL1/CX_3CR1 interaction in advanced and relapsed ovarian carcinoma metastasis. Our data indicate that the fractalkine axis regulates development and growth of lesions at peritoneal wall, diaphragm, liver, and kidney, i.e. sites commonly colonized by the relapsed disease. Further, our data indicate that the stromal CX_3CL1 plays a prominent role by supporting cell proliferation, as the tumor burden at organs in which CX_3CL1 expression was higher than that in tumors themselves was the most sensitive to downregulation of CX_3CR1 in the cancer cells. A major clinical challenge in the successful treatment of ovarian carcinoma is posed by the advanced and relapsed peritoneal metastasis characterized by rampant expansion, uncontrolled proliferation, and chemotherapy resistance, leading to patients' death (9, 47). Optimal debulking of peritoneal metastases carries significant survival benefits, suggesting that optimization of therapeutic approaches focused on reduction of the residual tumor burden will extend survival (48). Our studies indicate that downregulation of CX_3CR1 expression could significantly reduce both formation and growth of recurrent peritoneal lesions, thus providing rational for targeting the fractalkine axis in treatment of ovarian carcinoma.

Importantly, we found a significant correlation between the levels of CX_3CR1 expression and patients' survival, supporting a major role for the fractalkine axis in the aggressiveness of ovarian carcinoma.

Taken together, our data indicate that CX_3CR1 is a key regulator of formation and relapse of peritoneal metastasis in ovarian carcinoma. Not only that its high expression correlates with worse prognosis in postmenopausal patients at advanced and terminal disease stages, but CX_3CR1 could also play an active role in seeding secondary lesions as well as promoting metastasis by supporting CX_3CL1-dependent organ-specific metastatic growth. These data suggest that CX_3CR1 could be an optimal target for the retardation of metastatic expansion, leading to increasing survival, by negatively affecting multiple aspects of the peritoneal metastatic disease, from preventing recolonization to blocking metastatic growth at main sites relevant to the relapsed metastatic disease. At least a quarter of patients with serous ovarian carcinoma express CX_3CR1 at high levels that correlate with significantly shorter survival. This represents a large fraction of patients potentially benefitting from such a treatment, considering the high degree of molecular heterogeneity commonly displayed by this disease. Furthermore, our previous studies demonstrated that CX_3CR1 is expressed in all tested histotypes of epithelial and non-epithelial ovarian carcinoma, suggesting that

metastatic progression of all types of ovarian carcinoma may depend on CX_3CR1. Given that the ID8 cell culture model used in this study has been derived from murine ovarian surface epithelium, future studies involving models representing other histotypes of ovarian carcinoma are needed to firmly establish the role of CX_3CR1 in peritoneal adhesion and growth of metastatic lesions as it pertains to all types of ovarian carcinoma. The fractalkine axis has been shown to support a very limited number of normal physiological processes, including conception, regulation of resident macrophage population in the intestine, and glia-neuron interaction in the brain, negative effect on which could be managed (32, 49, 50). Encouragingly, a handful of CX_3CR1 targeting agents has been developed and successfully applied using various preclinical models (37, 39, 51). Given the results of our studies indicating a key role for CX_3CR1 in tumor growth and organ-specific peritoneal colonization, further studies are needed to assess the potential efficacy of these agents in metastatic ovarian carcinoma.

Materials and Methods

Materials

Mouse-derived ovarian carcinoma cell line ID8 (REF) was obtained from Dr. Katherine Roby (University of Kansas Medical Center) and maintained in minimal essential media supplemented with 10% fetal bovine serum. The cell line was cultured for no longer than 15 consecutive passages and was routinely assessed by cell morphology and the average doubling time. IMPACT III PCR profiling test (IDEXX RADIL) showed that the cell line was free of contamination by *Mycoplasma* spp., *Mycoplasma pulmonis*, mouse hepatitis virus, minute virus of mice, mouse parvovirus, Theiler's murine encephalomyelitis virus, Sendai virus, pneumonia virus of mice, murine norovirus, reovirus 3, mouse rotavirus, Ectromelia virus, Lymphocytic choriomeningitis virus, polyomavirus, and lactate dehydrogenase-elevating virus. Human ascites-derived ovarian adenocarcinoma cell line SKOV-3 was obtained from the NCI Tumor Bank Repository and maintained in minimal essential media supplemented with 10% fetal bovine serum. The cell line was cultured for no longer than 10 consecutive passages and was routinely assessed by cell morphology and the average doubling time; a Short Tandem Repeat (STR) analysis of this cell line revealed a 100% match to the DNA profile of SKOV-3 at ATCC. Four unique 29-mer CX_3CR1 (mouse)-specific shRNA constructs (#1 5'AGTGCAGCACGGTGTCACCATTAGTCTGG3', #2 5'GCCTTTGGAACCATCTTCCTGTCCGTCTT3', #3 5'AGTGGCGTTCAGCCACTGTTGCCTCAACC3', #4 5'CGTGCTCCGCAACTCGGAAGTCAACATCC3') and non-effective 29-mer scrambled shRNA cassette (5'GCACTACCAGAGCTAACTCAGATAGTACT3') in retroviral untagged vector were obtained from Origene. Six- to eight-weeks old C57BL/6 and athymic nude (FOXN1NU) mice were purchased from Jackson Laboratories (Sacramento, CA) and maintained at the AAALAC-approved animal facility at UIC in accordance with approved IACUC protocols. Tissue microarrays (TMA) containing human specimens of normal lymph node (LY481), normal kidney (KD803), normal liver (LVN241), and a single specimen of normal epiploon (greater omentum) from a healthy female were obtained from US Biomax (Rockville, MD). TMA containing normal human intestinal and stomach mesothelium

(GIP541) was obtained from Pantomics (Richmond, CA). Anti-CX_3CL1, anti-CX_3CR1, anti-rabbit, and anti-mouse biotin-conjugated antibodies were obtained from Abcam (Cambridge, MS). Anti-Ki67, anti-PCNA, and anti-CD95 antibodies were obtained from Novus Biologicals (Littleton, CO), Santa Cruz Biotechnologies (Dallas, TX), and BioLegend (San Diego, CA), respectively. ABC and DAB kits as well as animal-free blocker were obtained from Vector Laboratories (Burlingame, AL). DharmaFECT was obtained from Dharmacon (Lafayette, CO). Monoclonal anti-β-tubulin antibody was purchased from the Developmental Studies Hybridoma Bank (East Iowa City, IA). Transwell cell migration chambers with eight-micron pores were purchased from Corning (Corning, NY). CX3CR1 antagonist 18a (37) was purchased from Axon Medchem (Reston, VA). The WST-1 proliferation kit was obtained from Takara Bio (Madison, WI).

Short-term in vivo cell adhesion

10^6 cells of GFP-labeled parental ID8 and its subclones scr sh, cx2, and cx4 suspended in PBS in a total volume of 150 μl were i.p. injected into abdominal cavities of 6–8 weeks old female C57BL/6 mice (n=5). Animals were sacrificed 4 hours post injection following dissection of abdominal organs and tissues. Adhered fluorescent cells were visualized using inverted Axiovert Zeiss fluorescence microscope and enumerated.

Long-term tumor formation

For generation of intraperitoneal tumors 10^6 cells of parental ID8 and its subclones stably expressing CX_3CR1shRNA (clones cx2, cx3, cx4, and cx6) and scrambled shRNA suspended in PBS in a total volume of 150 μl were injected intraperitoneally (i.p.) into 6–8 weeks old female C57BL/6 mice (n=10). Sample size was chosen based on our previous *in vivo* studies (52, 53). Animals were randomly assigned to either control or experimental groups. In vivo experiments were performed by H.G.M. and J.X., who were blinded to the outcomes of the study. Animals were monitored three times weekly until they reached humane endpoints. Animals were sacrificed due to their poor health condition, a large volume of ascites, or 20% higher weight compared to the control group (animals injected with PBS). One animal in the “PBS” group was excluded due to malocclusion. Ascitic fluid was collected and measured. Animals were sacrificed, dissected, and the abdominal region was examined for visible tumors. Tumors associated with a specific organ were excised, measured, preserved in paraffin and examined by immunohistochemistry with hematoxylin&eosin (H&E).

Western blot and immunofluorescence staining

Western blot was used to detect the expression of CX_3CR1, CX_3CL1, and β-tubulin as previously described [38,39,41]. Immunofluorescence staining and imaging was performed as previously described (REF).

Immunohistochemical staining and scoring

Procedures were performed as we described before [43,46,47]. Briefly, slides containing paraffin-preserved human tissue sections were rehydrated by incubation in xylenes and ethanol solutions followed by blocking of peroxidase activity. Antigen retrieval was

achieved with a 10-min microwaving in 10 mM tris(hydroxymethyl)aminomethane (TRIS), 1 mM ethylenediaminetetraacetic acid (EDTA), pH 9.0. Primary mouse anti-human-CX_3CL1 antibody was used at 1 μg/ml overnight at 4 °C. Biotin-conjugated goat anti-mouse secondary antibodies were used at a dilution of 1:200 for 30 min at RT. Vectashield ABC and DAB reagent were prepared and used as suggested by the manufacturer. Slides were stained with hematoxylin, dehydrated, and mounted with Permount. Specimens of adrenal gland and ovarian carcinoma were used as a positive control, and exclusion of primary antibody was used as a negative control. Staining was evaluated by A.A.K.-B., O.E., and H.X., who were blinded to the experimental outcomes of the study. Staining was scored based on the intensity and percentage of positive cells as follows: “0” for negative cases, “1” for weakly positive cases, “2” for moderately positive cases, and “3” for highly positive cases. Staining was assessed in the membrane, the cytoplasm, and the nucleus.

Statistical analyses

For analyses of survival two non-parametric tests, the log-rank (Mantel-Cox) test and the Gehan-Breslow-Wilcoxon test, were employed using GraphPad Prism software. Comparisons between two data sets with normal distribution were conducted using Student’s t-test and Microsoft Excel software. Mann-Whitney U test and Tukey HSD test were used to compare two data sets with abnormal distribution. Data belonging to three or more independent groups were analysed using one-way ANOVA. The findings were considered statistically significant at $p<0.05$.

Supplementary Material

Refer to Web version on PubMed Central for supplementary material.

Acknowledgments

We thank Drs. William Beck, Joanna Burdette, Jonna Frasor, and Peter Penzes for their helpful suggestions on various methods and data analysis as well as critical reading of the manuscript. This study was supported by the National Cancer Institute (grant # CA160917 to MVB), and Ovarian Cancer Research Foundation Liz Tilberis Scholar Award (to MVB).

References

1. Auersperg N. The origin of ovarian carcinomas: a unifying hypothesis. Int J Gynecol Pathol. 2011; 30(1):12–21. [PubMed: 21131839]
2. Crum CP, Herfs M, Ning G, Bijron JG, Howitt BE, Jimenez CA, et al. Through the glass darkly: intraepithelial neoplasia, top-down differentiation, and the road to ovarian cancer. J Pathol. 2013; 231(4):402–412. [PubMed: 24030860]
3. Dubeau L. The cell of origin of ovarian epithelial tumours. The lancet oncology. 2008; 9(12):1191–1197. [PubMed: 19038766]
4. Dubeau L, Drapkin R. Coming into focus: the nonovarian origins of ovarian cancer. Ann Oncol. 2013; 24(Suppl 8):viii28–viii35. [PubMed: 24131966]
5. Kurman RJ. Origin and molecular pathogenesis of ovarian high-grade serous carcinoma. Ann Oncol. 2013; 24(Suppl 10):x16–x21. [PubMed: 24265397]
6. Siegel RL, Miller KD, Jemal A. Cancer statistics, 2016. CA Cancer J Clin. 2016; 66(1):7–30. [PubMed: 26742998]

7. Vaughan S, Coward JI, Bast RC Jr, Berchuck A, Berek JS, Brenton JD, et al. Rethinking ovarian cancer: recommendations for improving outcomes. Nat Rev Cancer. 2011; 11(10):719–725. [PubMed: 21941283]
8. Bowtell DD, Bohm S, Ahmed AA, Aspuria PJ, Bast RC Jr, Beral V, et al. Rethinking ovarian cancer II: reducing mortality from high-grade serous ovarian cancer. Nat Rev Cancer. 2015; 15(11):668–679. [PubMed: 26493647]
9. Lengyel E. Ovarian cancer development and metastasis. Am J Pathol. 2010; 177(3):1053–1064. [PubMed: 20651229]
10. Chang SJ, Bristow RE, Chi DS, Cliby WA. Role of aggressive surgical cytoreduction in advanced ovarian cancer. Journal of gynecologic oncology. 2015; 26(4):336–342. [PubMed: 26197773]
11. Pomel C, Jeyarajah A, Oram D, Shepherd J, Milliken D, Dauplat J, et al. Cytoreductive surgery in ovarian cancer. Cancer Imaging. 2007; 7:210–215. [PubMed: 18083650]
12. Seward SM, Winer I. Primary debulking surgery and neoadjuvant chemotherapy in the treatment of advanced epithelial ovarian carcinoma. Cancer Metastasis Rev. 2015; 34(1):5–10. [PubMed: 25597035]
13. Bookman MA. First-line chemotherapy in epithelial ovarian cancer. Clinical obstetrics and gynecology. 2012; 55(1):96–113. [PubMed: 22343232]
14. Colombo PE, Fabbro M, Theillet C, Bibeau F, Rouanet P, Ray-Coquard I. Sensitivity and resistance to treatment in the primary management of epithelial ovarian cancer. Critical reviews in oncology/hematology. 2014; 89(2):207–216. [PubMed: 24071502]
15. Davis A, Tinker AV, Friedlander M. "Platinum resistant" ovarian cancer: what is it, who to treat and how to measure benefit? Gynecol Oncol. 2014; 133(3):624–631. [PubMed: 24607285]
16. Wiedemeyer WR, Beach JA, Karlan BY. Reversing Platinum Resistance in High-Grade Serous Ovarian Carcinoma: Targeting BRCA and the Homologous Recombination System. Frontiers in oncology. 2014; 4:34. [PubMed: 24624361]
17. Thibault B, Castells M, Delord JP, Couderc B. Ovarian cancer microenvironment: implications for cancer dissemination and chemoresistance acquisition. Cancer Metastasis Rev. 2014; 33(1):17–39. [PubMed: 24357056]
18. Vanneman M, Dranoff G. Combining immunotherapy and targeted therapies in cancer treatment. Nat Rev Cancer. 2012; 12(4):237–251. [PubMed: 22437869]
19. Kim M, Rooper L, Xie J, Kajdacsy-Balla AA, Barbolina MV. Fractalkine receptor CX(3)CR1 is expressed in epithelial ovarian carcinoma cells and required for motility and adhesion to peritoneal mesothelial cells. Mol Cancer Res. 2012; 10(1):11–24. [PubMed: 22064656]
20. Gaudin F, Nasreddine S, Donnadieu AC, Emilie D, Combadiere C, Prevot S, et al. Identification of the chemokine CX3CL1 as a new regulator of malignant cell proliferation in epithelial ovarian cancer. PloS one. 2011; 6(7):e21546. [PubMed: 21750716]
21. Gurler H, Macias V, Kajdacsy-Balla AA, Barbolina MV. Examination of the Fractalkine and Fractalkine Receptor Expression in Fallopian Adenocarcinoma Reveals Differences When Compared to Ovarian Carcinoma. Biomolecules. 2015; 5(4):3438–3447. [PubMed: 26633537]
22. Rooper L, Gurler H, Kajdacsy-Balla AA, Barbolina MV. Fractalkine receptor is expressed in mature ovarian teratomas and required for epidermal lineage differentiation. Journal of ovarian research. 2013; 6(1):57. [PubMed: 23958497]
23. Balkwill F. Cancer and the chemokine network. Nat Rev Cancer. 2004; 4(7):540–550. [PubMed: 15229479]
24. Mantovani A, Savino B, Locati M, Zammataro L, Allavena P, Bonecchi R. The chemokine system in cancer biology and therapy. Cytokine & growth factor reviews. 2009; 21(1):27–39. [PubMed: 20004131]
25. Proudfoot AE. Chemokine receptors: multifaceted therapeutic targets. Nat Rev Immunol. 2002; 2(2):106–115. [PubMed: 11910892]
26. Tautermann CS. GPCR structures in drug design, emerging opportunities with new structures. Bioorganic & medicinal chemistry letters. 2014; 24(17):4073–4079. [PubMed: 25086683]
27. Combadiere C, Salzwedel K, Smith ED, Tiffany HL, Berger EA, Murphy PM. Identification of CX3CR1. A chemotactic receptor for the human CX3C chemokine fractalkine and a fusion coreceptor for HIV-1. J Biol Chem. 1998; 273(37):23799–2804. [PubMed: 9726990]

28. Imai T, Hieshima K, Haskell C, Baba M, Nagira M, Nishimura M, et al. Identification and molecular characterization of fractalkine receptor CX3CR1, which mediates both leukocyte migration and adhesion. Cell. 1997; 91(4):521–530. [PubMed: 9390561]
29. Bazan JF, Bacon KB, Hardiman G, Wang W, Soo K, Rossi D, et al. A new class of membrane-bound chemokine with a CX3C motif. Nature. 1997; 385(6617):640–644. [PubMed: 9024663]
30. Hundhausen C, Misztela D, Berkhout TA, Broadway N, Saftig P, Reiss K, et al. The disintegrin-like metalloproteinase ADAM10 is involved in constitutive cleavage of CX3CL1 (fractalkine) and regulates CX3CL1-mediated cell-cell adhesion. Blood. 2003; 102(4):1186–1195. [PubMed: 12714508]
31. Tsou CL, Haskell CA, Charo IF. Tumor necrosis factor-alpha-converting enzyme mediates the inducible cleavage of fractalkine. J Biol Chem. 2001; 276(48):44622–44626. [PubMed: 11571300]
32. Harrison JK, Jiang Y, Chen S, Xia Y, Maciejewski D, McNamara RK, et al. Role for neuronally derived fractalkine in mediating interactions between neurons and CX3CR1-expressing microglia. Proc Natl Acad Sci U S A. 1998; 95(18):10896–10901. [PubMed: 9724801]
33. Jamieson WL, Shimizu S, D'Ambrosio JA, Meucci O, Fatatis A. CX3CR1 is expressed by prostate epithelial cells and androgens regulate the levels of CX3CL1/fractalkine in the bone marrow: potential role in prostate cancer bone tropism. Cancer Res. 2008; 68(6):1715–1722. [PubMed: 18339851]
34. Jamieson-Gladney WL, Zhang Y, Fong AM, Meucci O, Fatatis A. The chemokine receptor CX(3)CR1 is directly involved in the arrest of breast cancer cells to the skeleton. Breast Cancer Res. 2011; 13(5):R91. [PubMed: 21933397]
35. Marchesi F, Piemonti L, Fedele G, Destro A, Roncalli M, Albarello L, et al. The chemokine receptor CX3CR1 is involved in the neural tropism and malignant behavior of pancreatic ductal adenocarcinoma. Cancer Res. 2008; 68(21):9060–9069. [PubMed: 18974152]
36. Shulby SA, Dolloff NG, Stearns ME, Meucci O, Fatatis A. CX3CR1-fractalkine expression regulates cellular mechanisms involved in adhesion, migration, and survival of human prostate cancer cells. Cancer Res. 2004; 64(14):4693–4698. [PubMed: 15256432]
37. Karlstrom S, Nordvall G, Sohn D, Hettman A, Turek D, Ahlin K, et al. Substituted 7-amino-5-thio-thiazolo[4,5-d]pyrimidines as potent and selective antagonists of the fractalkine receptor (CX3CR1). Journal of medicinal chemistry. 2013; 56(8):3177–3190. [PubMed: 23516963]
38. Ridderstad Wollberg A, Ericsson-Dahlstrand A, Jureus A, Ekerot P, Simon S, Nilsson M, et al. Pharmacological inhibition of the chemokine receptor CX3CR1 attenuates disease in a chronic-relapsing rat model for multiple sclerosis. Proc Natl Acad Sci U S A. 2014; 111(14):5409–5414. [PubMed: 24706865]
39. Shen F, Zhang Y, Jernigan DL, Feng X, Yan J, Garcia FU, et al. Novel Small-molecule CX3CR1 Antagonist Impairs Metastatic Seeding and Colonization of Breast Cancer Cells. Mol Cancer Res. 2016
40. Oncomine [Internet]. ThermoFisher Scientific. 2016 Jan. [cited January 2016] Available from: www.oncomine.org.
41. Roby KF, Taylor CC, Sweetwood JP, Cheng Y, Pace JL, Tawfik O, et al. Development of a syngeneic mouse model for events related to ovarian cancer. Carcinogenesis. 2000; 21(4):585–591. [PubMed: 10753190]
42. Walton J, Blagih J, Ennis D, Leung E, Dowson S, Farquharson M, et al. CRISPR/Cas9-Mediated Trp53 and Brca2 Knockout to Generate Improved Murine Models of Ovarian High-Grade Serous Carcinoma. Cancer Res. 2016; 76(20):6118–6129. [PubMed: 27530326]
43. Burleson KM, Hansen LK, Skubitz AP. Ovarian carcinoma spheroids disaggregate on type I collagen and invade live human mesothelial cell monolayers. Clinical & Experimental Metastasis. 2004; 21(8):685–697. [PubMed: 16035613]
44. Iwanicki MP, Davidowitz RA, Ng MR, Besser A, Muranen T, Merritt M, et al. Ovarian cancer spheroids use myosin-generated force to clear the mesothelium. Cancer discovery. 2011; 1(2):144–157. [PubMed: 22303516]
45. Tsubota K, Nishiyama T, Mishima K, Inoue H, Doi T, Hattori Y, et al. The role of fractalkine as an accelerating factor on the autoimmune exocrinopathy in mice. Invest Ophthalmol Vis Sci. 2009; 50(10):4753–4760. [PubMed: 19407023]

46. Erreni M, Siddiqui I, Marelli G, Grizzi F, Bianchi P, Morone D, et al. The Fractalkine-Receptor Axis Improves Human Colorectal Cancer Prognosis by Limiting Tumor Metastatic Dissemination. J Immunol. 2015; 196(2):902–914. [PubMed: 26673138]

47. Matulonis UA, Sood AK, Fallowfield L, Howitt BE, Sehouli J, Karlan BY. Ovarian cancer. Nat Rev Dis Primers. 2016; 2:16061. [PubMed: 27558151]

48. Chi DS, Musa F, Dao F, Zivanovic O, Sonoda Y, Leitao MM, et al. An analysis of patients with bulky advanced stage ovarian, tubal, and peritoneal carcinoma treated with primary debulking surgery (PDS) during an identical time period as the randomized EORTC-NCIC trial of PDS vs neoadjuvant chemotherapy (NACT). Gynecol Oncol. 2012; 124(1):10–14. [PubMed: 21917306]

49. Medina-Contreras O, Geem D, Laur O, Williams IR, Lira SA, Nusrat A, et al. CX3CR1 regulates intestinal macrophage homeostasis, bacterial translocation, and colitogenic Th17 responses in mice. J Clin Invest. 2011; 121(12):4787–4795. [PubMed: 22045567]

50. Zhang Q, Shimoya K, Temma K, Kimura T, Tsujie T, Shioji M, et al. Expression of fractalkine in the Fallopian tube and of CX3CR1 in sperm. Human reproduction (Oxford, England). 2004; 19(2): 409–414.

51. Dorgham K, Ghadiri A, Hermand P, Rodero M, Poupel L, Iga M, et al. An engineered CX3CR1 antagonist endowed with anti-inflammatory activity. J Leukoc Biol. 2009; 86(4):903–911. [PubMed: 19571253]

52. Desjardins M, Xie J, Gurler H, Muralidhar GG, Sacks JD, Burdette JE, et al. Versican regulates metastasis of epithelial ovarian carcinoma cells and spheroids. Journal of ovarian research. 2014; 7:70. [PubMed: 24999371]

53. Kim M, Rooper L, Xie J, Rayahin J, Burdette JE, Kajdacsy-Balla A, et al. The Lymphotactin Receptor Is Expressed in Epithelial Ovarian Carcinoma and Contributes to Cell Migration and Proliferation. Mol Cancer Res. 2012

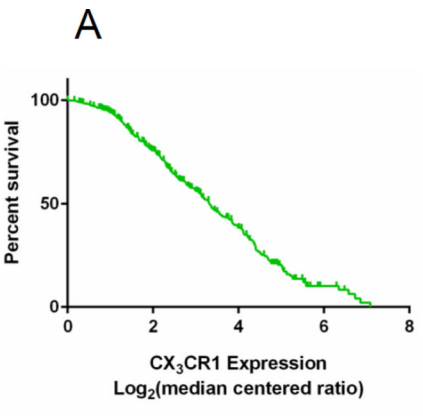

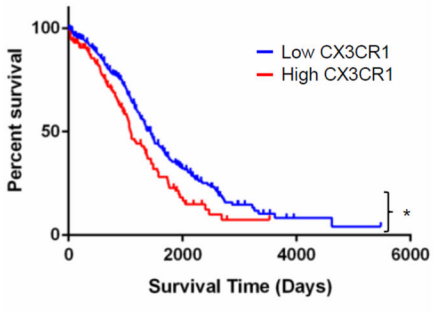

CX3CR1 status	Survival, days
High	1089
Low	1442

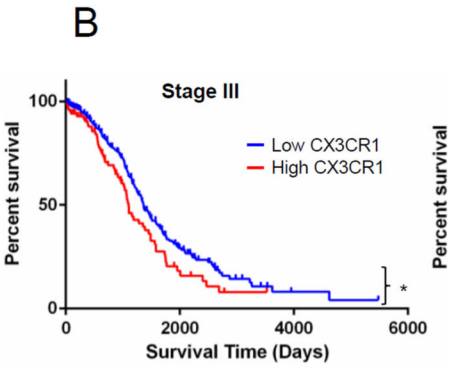

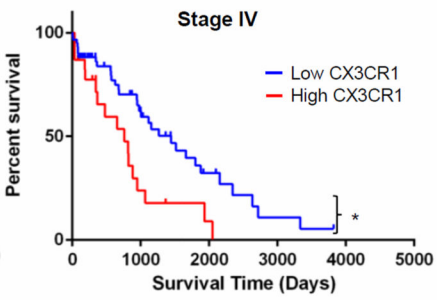

CX3CR1 status	Survival, days	
	Stage III	Stage IV
High	1102	759
Low	1364	1446

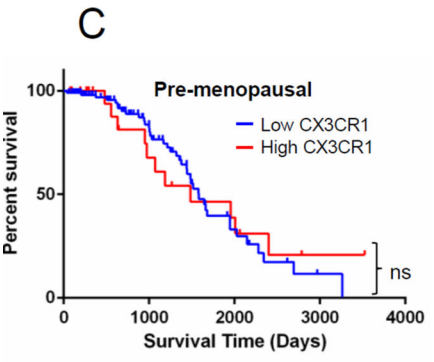

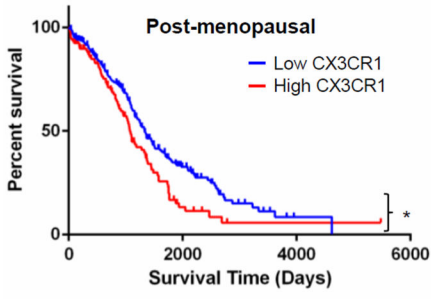

CX3CR1 status	Survival, days	
	Pre-meno	Post-meno
High	1583	1073
Low	1484	1336

FIGURE 1. High expression of CX_3CR1 correlates with an overall shorter survival

(A) High *vs* low CX_3CR1 expression predicts an overall shorter survival in patients with serous ovarian carcinoma. Data from The Cancer Genome Atlas (TCGA) database for serous ovarian adenocarcinoma were analysed in Oncomine and plotted as CX_3CR1 expression $Log_{2(\text{median centered ratio})}$ vs percent survival (green line; left panel). Data points with incomplete information were removed from the analysis; total number of specimens analysed was 557. Based on the value of median CX_3CR1 expression, defined as CX_3CR1 expression $Log_{2(\text{median centered ratio})}$ at 50% survival, the data set was divided in two (center

panel), including specimens with CX_3CR1 expression > 3.32, termed “high CX_3CR1 expression” (n=143; red line), and specimens with CX_3CR1 expression < 3.32, termed “low CX_3CR1 expression” (n=414; blue line). Overall survival of patients expressing high and low levels of CX_3CR1 was plotted and analysed with Kaplan-Meier plot using Prism software (center panel). Average overall survival of patients with high and low CX_3CR1 expression is indicated in the Table (right panel). *p=0.0020, Log-rank (Mantel-Cox) test; *p=0.0027, Gehan-Breslow-Wilcoxon test. **(B) High *vs* low CX_3CR1 expression predicts an overall shorter survival in patients with serous ovarian carcinoma at FIGO Stages III and IV**. The specimens in groups containing Stage III (n=429) and Stage IV (n=83) specimens were divided in two groups with “high” and “low” CX_3CR1 expression (red and blue lines, respectively) corresponding to cases with higher than median CX_3CR1 expression and lower than median CX_3CR1 expression, respectively (3.23 for Stage III and 3.77 for Stage IV). Overall survival of patients with Stage III disease expressing high (n=100) and low (n=329) levels of CX_3CR1 was plotted and analysed with Kaplan-Meier plot using Prism software (left panel); *p=0.0205, Log-rank (Mantel-Cox) test, *p=0.0170, Gehan-Breslow-Wilcoxon test. Overall survival of patients with Stage IV disease expressing high (n=23) and low (n=60) levels of CX_3CR1 was plotted and analysed with Kaplan-Meier plot using Prism software (center panel);*p=0.0036, Log-rank (Mantel-Cox) test, *p=0.0197, Gehan-Breslow-Wilcoxon test. Average overall survival of patients at Stage III and IV disease with high and low CX_3CR1 expression is indicated in the Table (right panel). **(C) High *vs* low CX_3CR1 expression predicts an overall shorter survival in postmenopausal patients with serous ovarian carcinoma**. Overall survival of patients of pre-menopausal age with high (n=22) and low (n=108) CX_3CR1 expression was plotted and analysed using Kaplan-Meier plots (left panel); p=0.8421, Log-rank (Mantel-Cox) test, p=0.5221, Gehan-Breslow-Wilcoxon test. Overall survival of patients of post-menopausal age with high (n=120) and low (n=307) CX_3CR1 expression was plotted and analysed using Kaplan-Meier plots (center panel); *p=0.0046, Log-rank (Mantel-Cox) test, *p=0.0215, Gehan-Breslow-Wilcoxon test. Average overall survival of patients of both pre- and post-menopausal age with high and low CX_3CR1 expression is indicated in the Table (right panel).

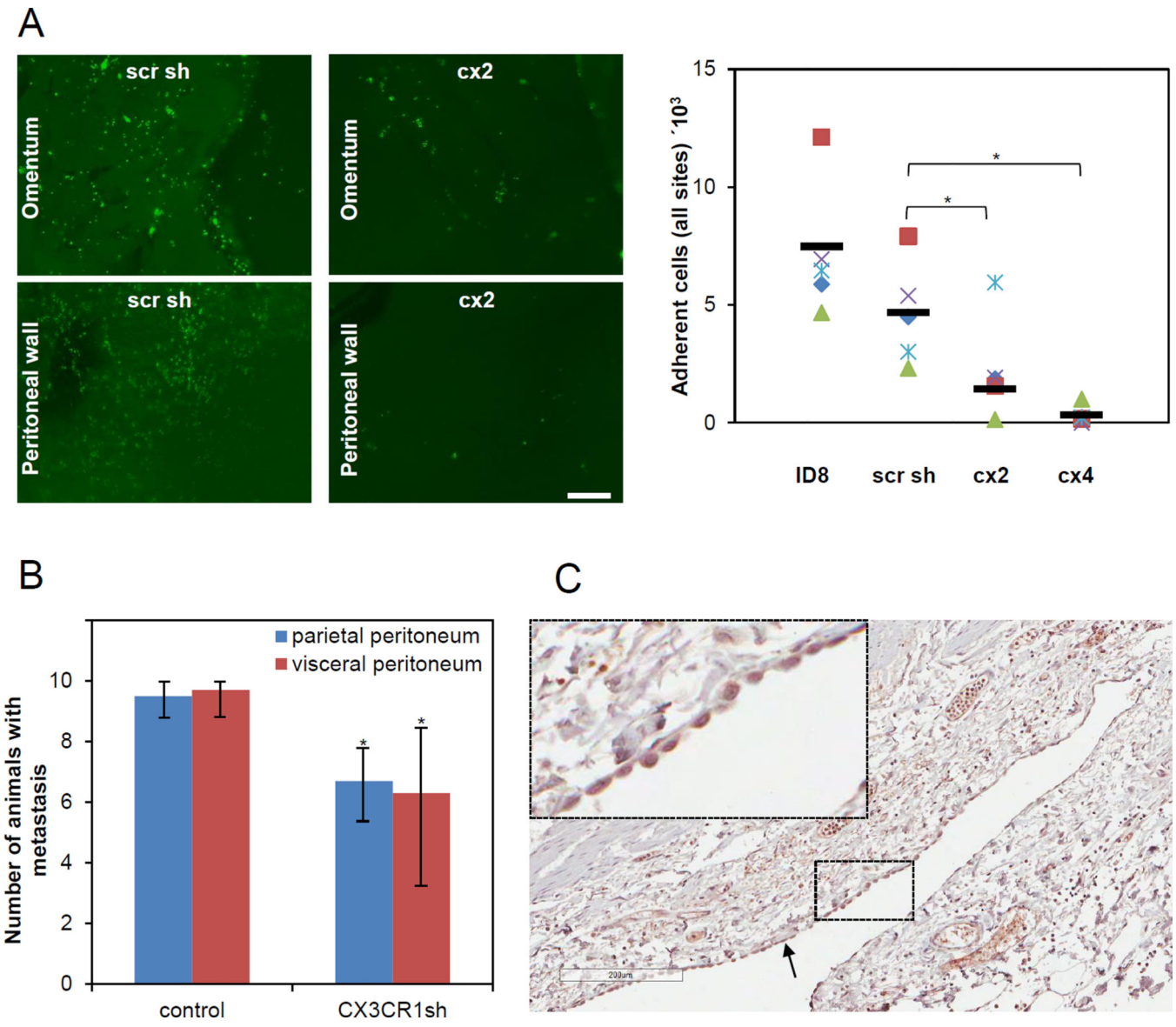

FIGURE 2. CX_3CR1 supports peritoneal adhesion and tumor formation in a syngeneic model of ovarian carcinoma

(A) Short-term *in vivo* adhesion assay demonstrates that CX_3CR1 is important for peritoneal adhesion. Immunofluorescence images (green fluorescence) demonstrate cells adherent to omentum and peritoneal wall, as indicated, 4 hours following i.p. injection of the GFP-labeled control (scr sh group) and experimental (cx2 clone) ID8 cells into abdomens of C57BL/6 (5/group). Adherent cells were visualized under the fluorescence microscope in tissues excised from sacrificed control (injected with ID8 and scr sh) and experimental (injected with cx2 and cx4 clones) animals, enumerated using Zeiss AxioVert software, and plotted. Red squares – mouse #1, purple checks – mouse #2, blue flakes – mouse #3, green triangles – mouse #4, blue diamonds – mouse #5. Bars show an average number of adherent cells in each group. The differences between groups (cx2 *vs* scr sh and cx4 *vs* scr sh) were statistically analysed using both Mann-Whitney U test and Students' t-test; * $p<0.05$.

Differences between ID8 and scr sh groups were not statistically significant using both Mann-Whitney U test and Students' t-test. All groups were statistically analysed using one-way ANOVA; p=0.0026. **(B) Downregulation of CX_3CR1 leads to significant reduction of tumor formation**. The number of animals bearing metastasis on the organs covered by the parietal peritoneum and the visceral peritoneum in both control (ID8 and scr sh combined to a total of 20 animals; designated "control") and experimental (clones cx2, cx3, and cx6 combined to a total of 30 animals; designated "CX_3CR1sh") groups was calculated and plotted. Animals were considered positive for metastasis at each site if lesions visible with the naked eye were present upon dissection when animals reached humane endpoints. The data are shown as average ± standard deviation and were statistically analyzed using Students' t-test.; * p<0.05. **(C) Normal human mesothelium is strongly CX_3CL1-positive**. Expression of CX_3CL1 in human mesothelium was determined using immunohistochemistry and anti-CX_3CL1-specific antibodies. A typical image of the CX_3CL1 immunostaining in normal mesothelium from intestine/colon of a 55 year old woman is shown (core B1, Supplementary Table 1). Black arrow points to the mesothelial monolayer. Brown, CX_3CL1; blue, hematoxylin. Bar, 200 micron. Insert is a 5-fold magnification of the area outlined with dashed lines.

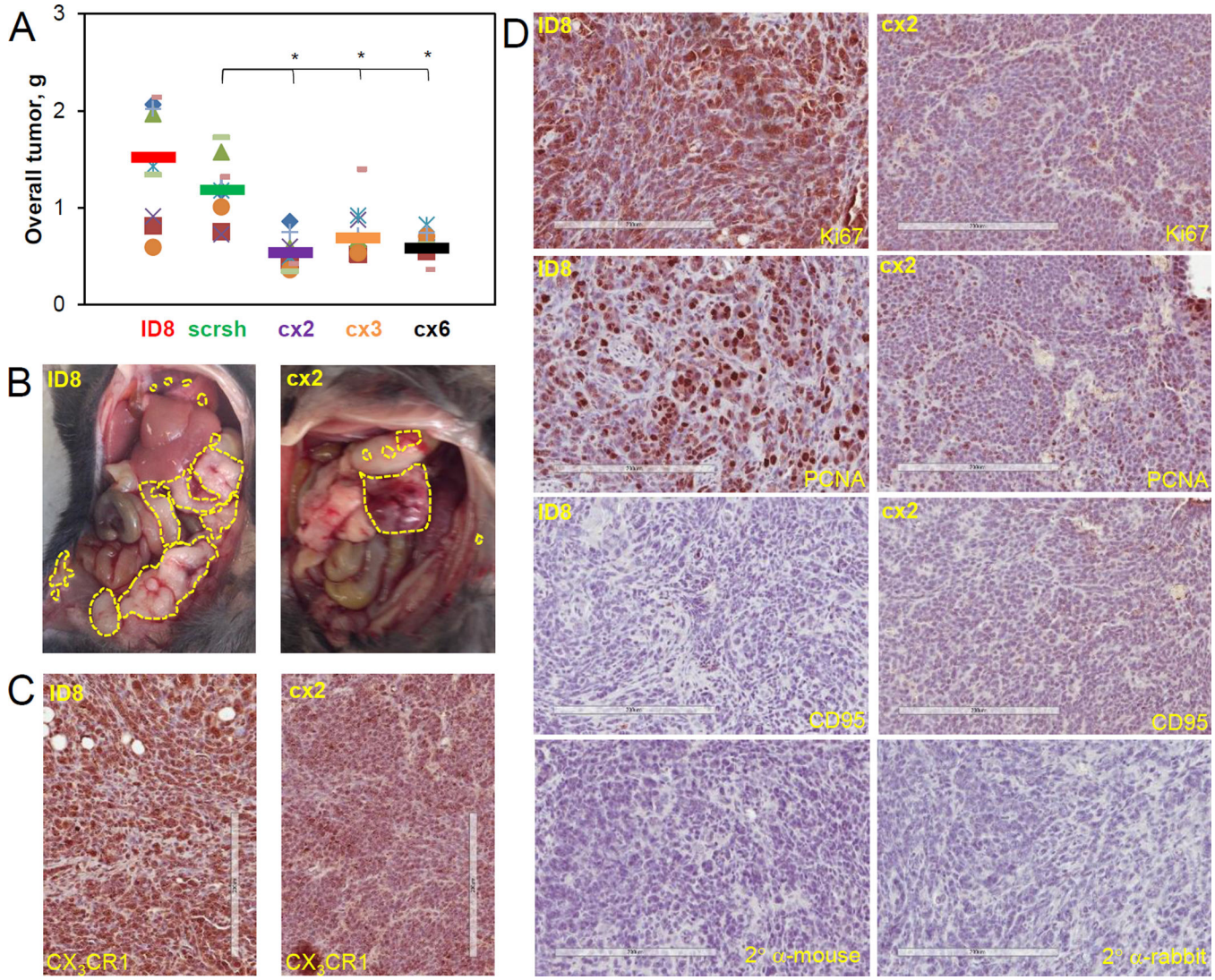

FIGURE 3. Downregulation of CX_3CR1 expression results in significantly reduced overall tumor burden in a syngeneic model of ovarian carcinoma

(**A**) An overall tumor burden was calculated by adding the weights of individual tumor nodules at all sites (omentum, peritoneal wall, diaphragm, liver, mesenthery, kidney, ovary&uterus, and pancreas) and plotted. Orange circles – mouse #1, red squares – mouse #2, purple checks – mouse #3, lime dashes – mouse #4, blue flakes – mouse #5, green triangles – mouse #6, green crosses – mouse #7, blue diamonds – mouse #8, orange dashes – mouse #9, lilac diamonds – mouse #10. Color coding for the control and experimental animal groups: red – ID8, green – scr sh, purple – cx2, orange – cx3, black– cx6. Bars show an average tumor burden in each group. Differences between two groups were analysed using both Mann-Whitney U test and Students' t-test; * $p<0.05$. All groups were statistically analysed using one-way ANOVA; $p=0.0030$. (**B**) Typical images of gross tumor dissemination throughout the abdomen for ID8 and CX2 groups are shown (bottom panels). Yellow dashed lines outline tumor nodules. Specimens of tumors generated by ID8 and CX2 groups at the time of sacrifice were immunohistochemically stained for CX_3CR1 (**C**) as well

as Ki67, PCNA, and CD95 (**D**). Primary antibody omission was used as negative control; sections were incubated with secondary anti-mouse and anti-rabit antibodies only, as indicated. Bar, 200 micron. Brown: CX_3CR1, Ki67, PCNA, or CD95, as indicated. Blue: hematoxylin.

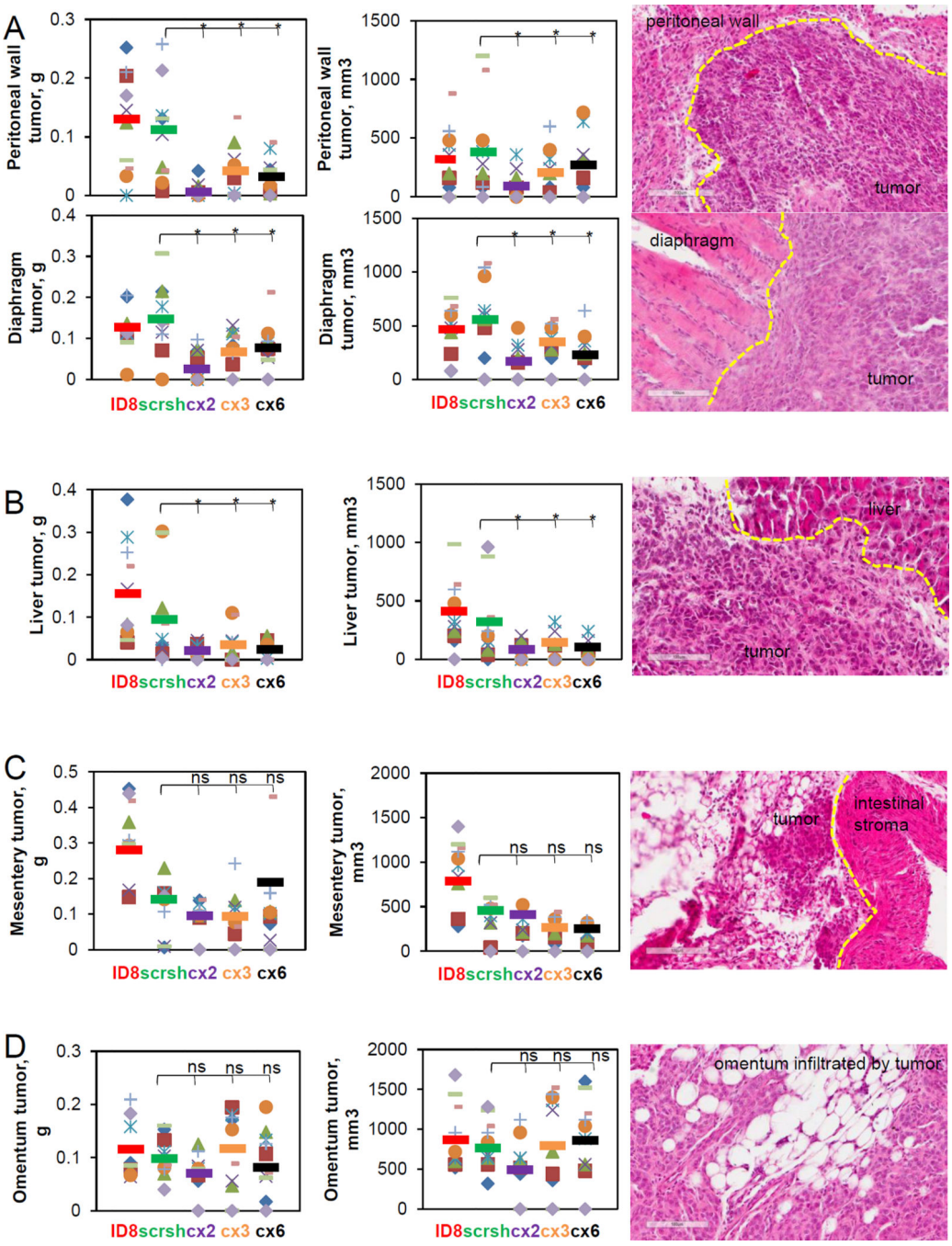

FIGURE 4. Effect of CX_3CR1 downregulation on development of intraperitoneal metastasis at (A) peritoneal wall and diaphragm, (B) liver, (C) the mesentery, and (D) the omentum

Tumors at each site were excised weighted, measured, and the results were plotted (left and center panels). Orange circles – mouse #1, red squares – mouse #2, purple checks – mouse #3, lime dashes – mouse #4, blue snowflakes – mouse #5, green triangles – mouse #6, green crosses – mouse #7, blue diamonds – mouse #8, orange dashes – mouse #9, lilac diamonds – mouse #10. Color coding for the control and experimental animal groups throughout the figure: red – ID8, green – scr sh, purple – cx2, orange – cx3, black– cx6. Bars show an average tumor burden in each group. Differences between two groups (scr sh and clones)

were analysed using both Mann-Whitney U test and Students' t-test; * $p<0.05$. Tumors were preserved, sectioned, and stained with hematoxylin and eosin. Dashed yellow lines separate tumors from stroma. Images were generated using Aperio ScanScope (right panels). Bar, 100 micron.

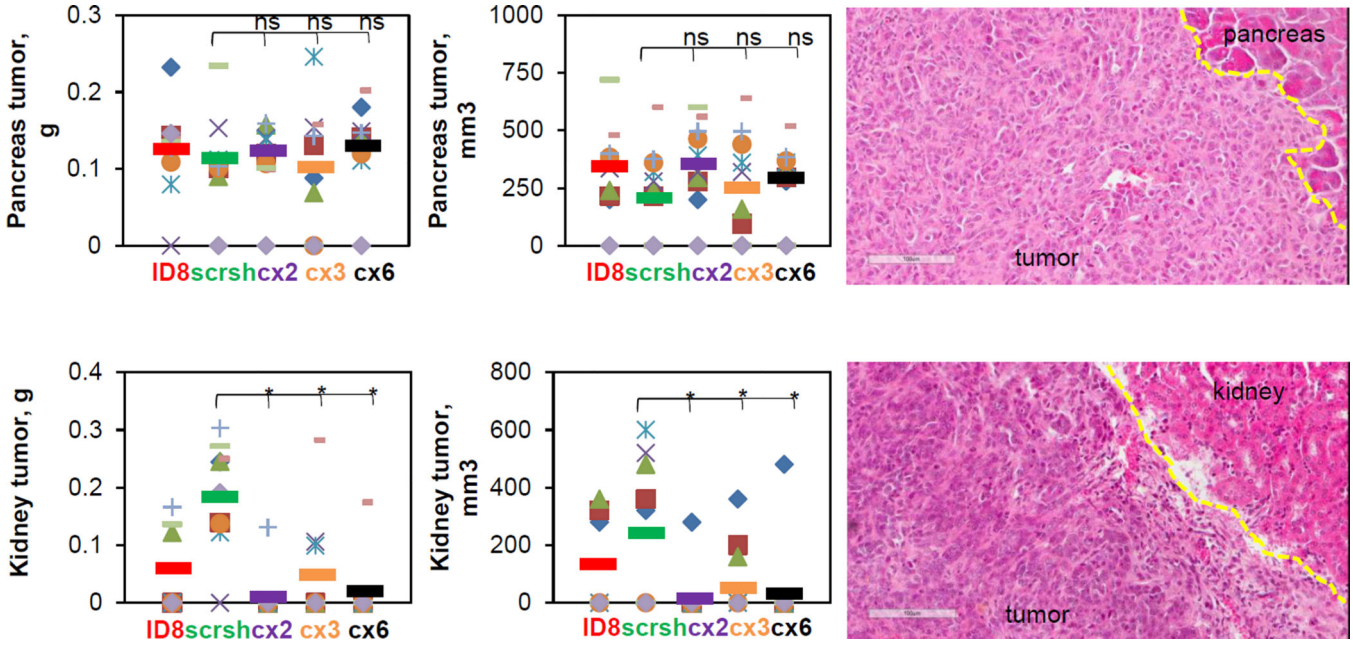

FIGURE 5. Effect of CX_3CR1 downregulation on development of retraperitoneal metastasis at pancreas and kidney

Tumors at each site were excised weighted, measured, and the results were plotted (left and center panels). Orange circles – mouse #1, red squares – mouse #2, purple checks – mouse #3, lime dashes – mouse #4, blue snowflakes – mouse #5, green triangles – mouse #6, green crosses – mouse #7, blue diamonds – mouse #8, orange dashes – mouse #9, lilac diamonds – mouse #10. Color coding for the control and experimental animal groups throughout the figure: red – ID8, green – scr sh, purple – cx2, orange – cx3, black– cx6. Bars show an average tumor burden in each group. Differences between two groups (scr sh and clones) were analysed using both Mann-Whitney U test and Students' t-test; * $p<0.05$. Tumors and outlying stromal regions were preserved, sectioned, and stained with hematoxylin and eosin. Dashed yellow lines separate tumors from stroma. Images were generated using Aperio ScanScope (right panels). Bar, 100 micron.

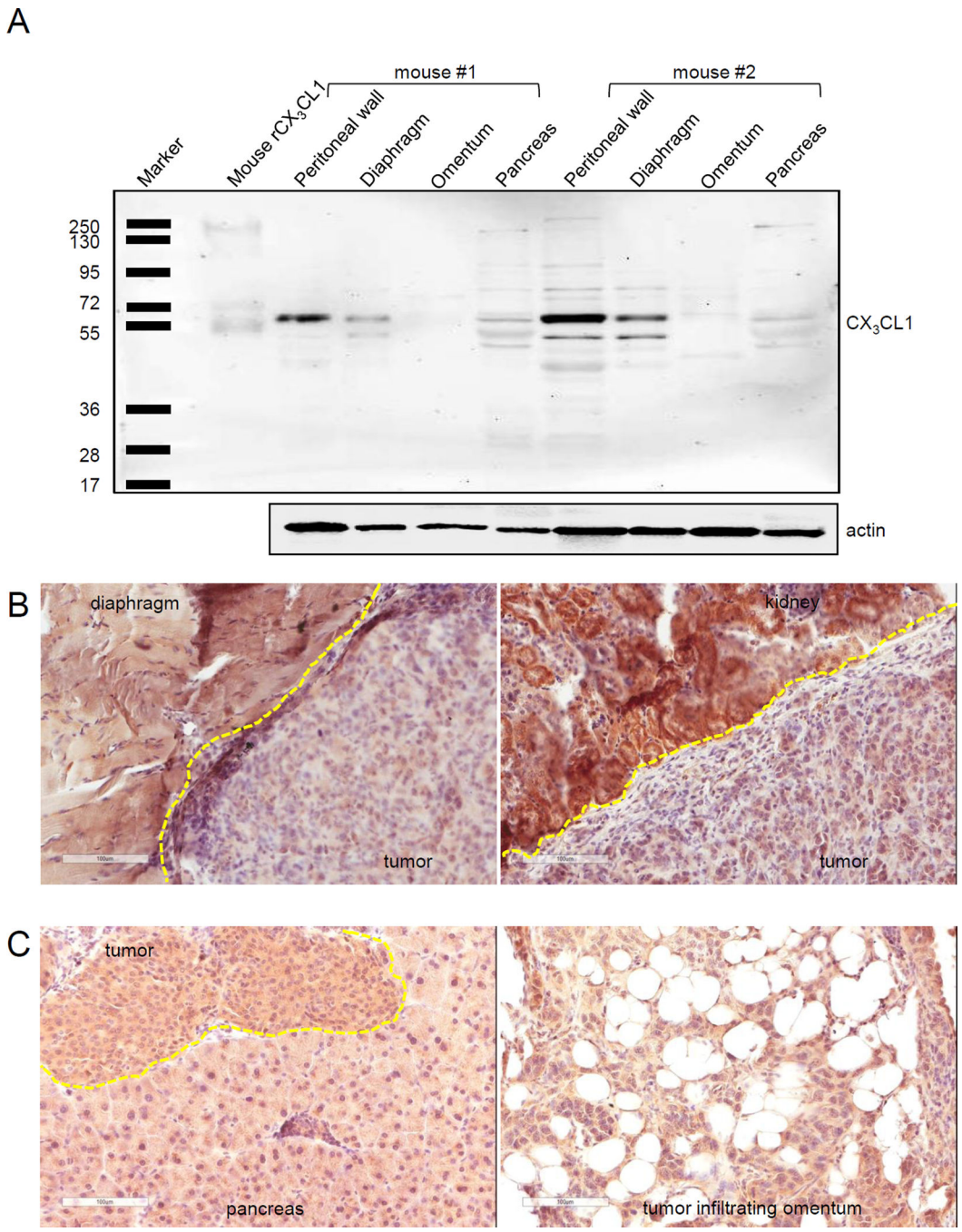

FIGURE 6. Role of tumoral and stromal CX_3CL1 in CX_3CR1-dependent metastatic dissemination

(A) Expression of CX_3CL1 in specimens of tumor-naive mouse omentum, pancreas, peritoneal wall, and diaphragm. Expression of CX_3CL1 in total cell lysates (10 μg protein/lane) of peritoneal wall, diaphragm, omentum, and pancreas obtained from tumor-naive C57BL/6 mice (n=2) was detected using Western blot. Left lane shows positions of the molecular weight marker proteins. Mouse recombinant CX_3CL1 (10 ng) served as a positive control. Actin served as a loading control. **(B,C) Tumoral and stromal CX_3CL1**

expression. CX_3CL1 in tumor and invaded stroma, as specified for each host site, was visualized with immunostaining in organ sites dissemination to which correlated with CX_3CR1 expression in tumor cells (diaphragm, kidney, (**B**)) and where it did not depend on CX_3CR1 expression in the tumor cells (pancreas, omentum, (**C**)). Images were generated using Aperio ScanScope; bar, 100 micron. Dashed yellow lines separate tumors from stroma. Brown, CX_3CL1; blue, hematoxylin.

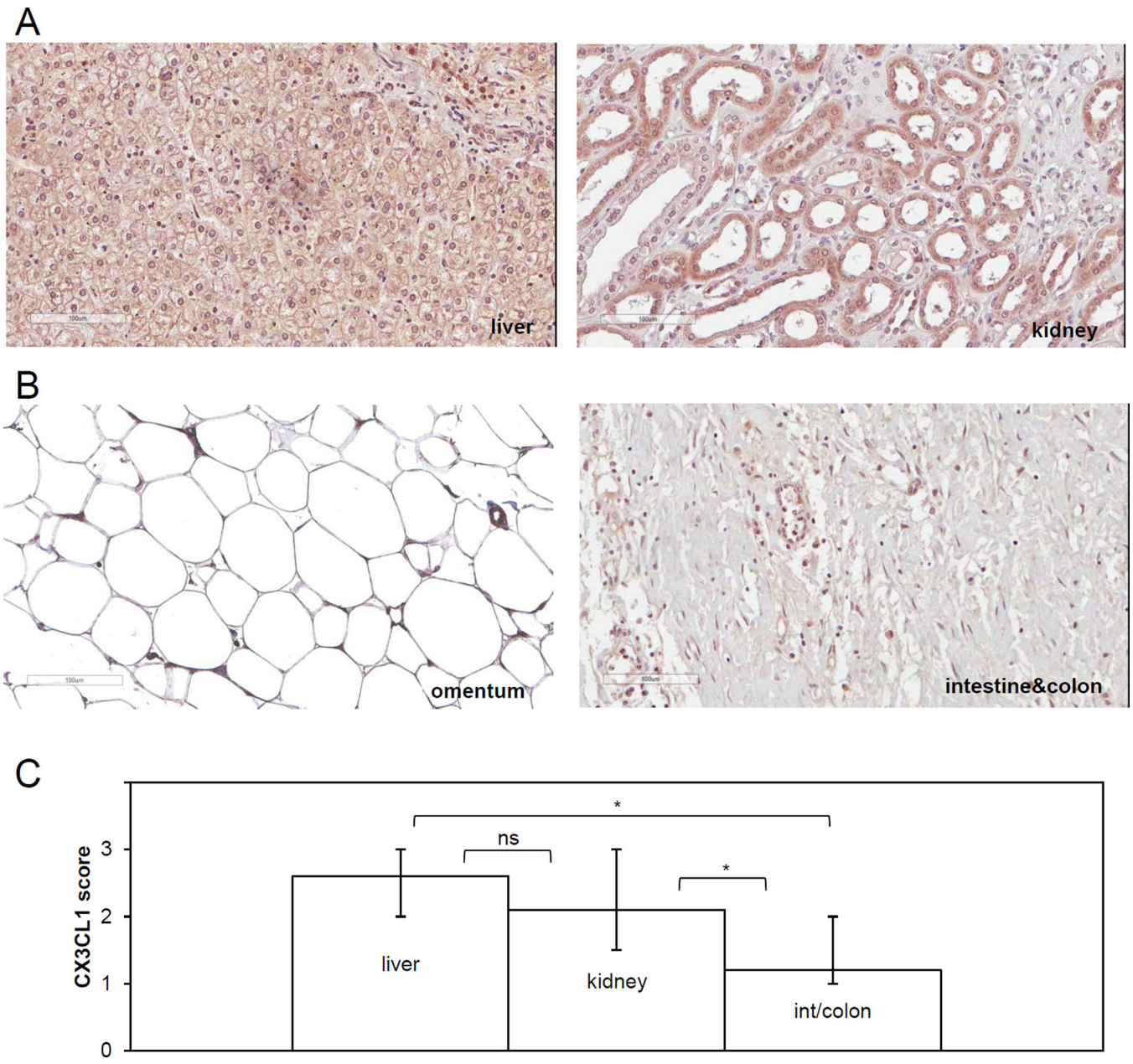

FIGURE 7. Expression of CX_3CL1 in human kidney and liver is higher compared to that in intestine/colon and omentum

Immunohistochemical staining with CX_3CL1-specific antibodies was used to determine CX_3CL1 expression and intracellular localization in normal human specimens of liver and kidney (**A**), intestine/colon, and omentum (**B**). Brown, CX_3CL1; blue, hematoxylin. Typical images of CX_3CL1-immunoreactive staining in specimens of liver, kidney, intestine/colon, and omentum are shown. Image of liver corresponds to the case C6 (Supplementary Table 3), image of kidney corresponds to the case A4 (Supplementary Table 4), image of intestine/colon corresponds to the case C06 (Supplementary Table 1) and image of normal human specimen of epiploon (greater omentum) belongs to a 21 year old female. Brown, CX_3CL1; blue, hematoxylin. Images were generated using Aperio ScanScope; bar, 100 micron. (**C**)

Comparison of the CX_3CL1 immunoscores among the tested tissues. The scoring was performed for the entire tissue, including all cell types present (of note, specimens of intestine/colon contained stroma underlying mesothelium, consistent with the microenvironment surrounding ovarian cancer cells anchoring in submesothelial stroma). The normal liver TMA contained 9 female and 15 male specimens; the average staining in female and male samples was 2.6 and 2.4, respectively (Supplementary Table 3). The normal kidney TMA contained 24 female and 56 male specimens; the average staining score in female and male samples was 2.1 and 2.3, respectively (Supplementary Table 4). Distal tubules displayed stronger immunoreactivity against CX_3CL1 antibodies compared to the proximal tubules. The visceral peritoneum TMA contained both stomach and intestine/colon specimens. Among those there were 13 female and 14 male intestine/colon specimens with average staining score of 1.2 and 1.0, respectively. Immunoscores of CX_3CL1 expression in female specimens of normal human liver, kidney, and intestine/colon were averaged and plotted. The data were analysed using both Mann-Whitney U test and Students' t-test; * $p<0.05$.